ACS APPLIED MATERIALS & INTERFACES

Research Article

www.acsami.org

Hierarchical ZnO Nanorods on Si Micropillar Arrays for Performance Enhancement of Piezoelectric Nanogenerators

Md Roqibul Hasan,[†,§] Seong-Ho Baek,[‡,§] Kwang Su Seong,[†] Jae Hyun Kim,*[,‡] and Il-Kyu Park*[,†]

[†]Department of Electronic Engineering, Yeungnam University, Gyeongbuk 712-749, South Korea

[‡]Energy Research Division, Daegu Gyeongbuk Institute of Science & Technology, Daegu 711-873, South Korea

Supporting Information

ABSTRACT: Enhanced output power from a ZnO nanorod (NR)-based piezoelectric nanogenerator (PNG) is demonstrated by forming a heterojunction with Si micropillar (MP) array. The length of the SiMP array, which was fabricated by electrochemical etching, was increased systematically from 5 to 20 μm by controlling the etching time. Our structural and optical investigations showed that the ZnO NRs were grown hierarchically on the SiMPs, and their crystalline quality was similar regardless of the length of the underlying SiMPs. The peak output voltage from the ZnO NR-based PNG was greatly increased by ~5.7 times, from 0.7 to 4.0 V, as the length of the SiMP arrays increased from 0 (flat substrate) to 20 μm. The enhancement mechanism was explained based on the series connection of the ZnO NRs regarded as a single source of piezoelectric potential by creating a heterojunction onto the SiMP arrays.

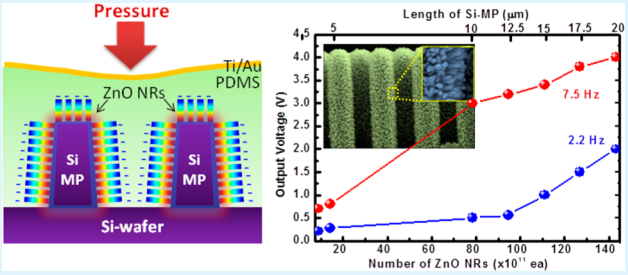

KEYWORDS: *ZnO nanorods, hierarchical nanostructures, heterojunction, piezoelectric nanogenerators*

1. INTRODUCTION

Recently, wireless sensor networks that integrate multifunctional nanodevices for sensing, controlling, actuating, responding, and communicating by themselves have received much attention for application to the Internet.[1−3] However, such a sensor network would be impractical if each device needed to be powered by conventional battery technologies.[1−3] Therefore, new sustainable self-powering sources that can scavenge energy from the environment are being examined.[4] Harvesting abundantly available wasted ambient mechanical energy (e.g., from human activity, machinery vibration, noise or sound waves, air flow, and water flow) has been a long-standing dream and is being widely investigated for use in sustainable and self-powering systems.[5−7] After the demonstration of the concept for the piezoelectric nanogenerator (PNG),[8] the theory, the fabrication technologies, and feasible applications for the PNGs have been widely investigated and developed to enhance the output power of PNGs.[9−13] Among the materials for PNG applications, ZnO has been the most widely used. This is because ZnO-based nanostructures can be easily fabricated on various materials, and its naturally asymmetric hexagonal wurtzite structure and its polar crystal surfaces give rise to superior piezoelectric properties.[8,12,14] In future applications, such as wireless sensor networks, the energy-harvesting devices should be integrated into Si-based technology for better compatibility with complementary metal oxide semiconductor (CMOS) technology. Using Si as a substrate for PNGs has many advantages including low cost, large area fabrication, and controllable doping, which enables them to be used as a conductive electrode and allows easier hybridization with other technologies, such as batteries and photovoltaics. In addition, a heterojunction of the n-ZnO/p-type materials is expected to be beneficial by reducing the free charge screening effects while preserving piezo charges.[15−17] However, even though many studies have investigated fabricating PNGs on flexible organic, textile, and other insulating substrates,[5−13] few investigations have reported the fabrication and performance enhancement of heterostructured PNGs on Si substrates.[18−20] Therefore, hybridizing these ZnO nanostructures and p-Si would be a synergetic way to enhance piezoelectric properties as well as realize a self-powering system. In this study, we report the fabrication and performance enhancement of heterostructured PNGs by combining ZnO nanorods (NRs) grown on length-controlled Si micropillar (SiMP) arrays using solution processes. Taking advantage of the ZnO NRs/SiMP heterojunction, excellent piezoelectric performances were obtained with increasing SiMP length and ZnO NR density.

2. EXPERIMENTAL DETAILS

2.1. Fabrication of Samples. The fabrication process for heterostructured ZnO NR PNGs on SiMP arrays is illustrated in Figure 1. SiMP arrays were prepared on boron-doped p-Si (100) wafers with a resistivity of 1 Ω cm by combining photolithography and electrochemical etching methods.[21] SiMP arrays with a length ranging from 5 to 20 μm were prepared on p-Si within a circular area with a diameter of 2.5 cm. A 5 nm thick ZnO thin film was deposited on the

Received: December 4, 2014
Accepted: January 26, 2015
Published: January 26, 2015

DOI: 10.1021/am5085379
ACS Appl. Mater. Interfaces 2015, 7, 5768−5774

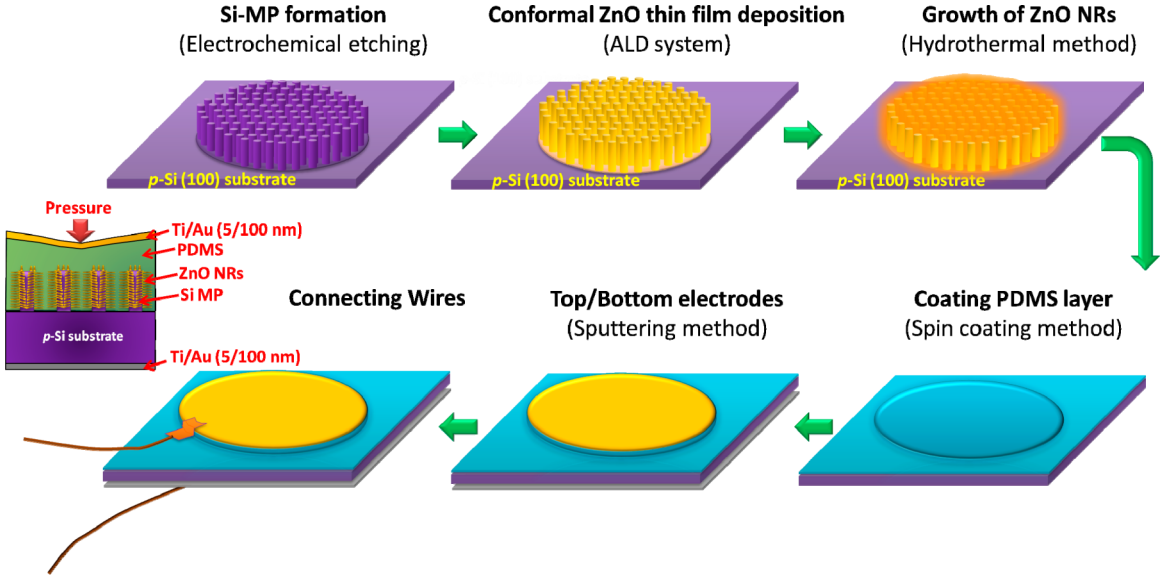

Figure 1. Schematic of processing steps for fabrication of ZnO NR-PNG on SiMP.

SiMP arrays as a seed layer using the atomic layer deposition (ALD) technique. The ALD method provides a conformal coating of ZnO deposits, even on complicated structures, because of a long mean free path, and fewer gas-phase reactions of the sources in the deposition system.[22] Under our optimal deposition conditions, the growth rate of the ZnO films was 1.5 to 1.6 angstroms/cycle at a substrate temperature of 200 °C. ZnO NRs were grown on the ZnO seed layer-grown SiMP arrays using the low-temperature hydrothermal method.[23] ZnO NRs were grown by placing the ZnO seed layer-deposited SiMP arrays into a mixed solution of 60 mM zinc nitrate hexahydrate ($Zn(NO_3)_2{\cdot}6H_2O$) and 60 mM hexamethylenetetramine ($(CH_2)_6N_4$) in deionized (DI) water at 90 °C for 2 h. After the reaction, the samples were cleaned in flowing DI water for 10 min to completely remove the residues from the samples, which can induce an electrical shortage during operation of the PNG. ZnO NRs were also prepared on flat p-Si substrate as a reference using the same process. After growing the ZnO NRs, a 10 μm thick polydimethylsiloxane (PDMS) layer was deposited on the SiMP arrays with ZnO NRs using the spin-coating method. PDMS prepolymer (Sylgard-184, Dow Corning, Midland, MI) was prepared by thoroughly mixing the PDMS curing agent with the PDMS base monomer at a weight ratio of 10:1. PDMS prepolymer was then spin-coated at 2000 rpm for 30 s on the ZnO NR layer-grown SiMP arrays and subsequently annealed at 70 °C for 30 min for curing. During the annealing process the samples were evacuated in a vacuum chamber to remove bubbles from the PDMS and to enhance the adhesion between the ZnO NRs and PDMS layers. A Ti/Au (5/100 nm) layer was then deposited to create top and bottom electrodes using a sputtering method.

2.2. Characterization and Measurement of Samples. The structural properties of ZnO NRs were investigated by field emission scanning electron microscopy (FE-SEM). The optical properties of the ZnO NRs were examined by photoluminescence (PL) spectroscopy, which were measured using a 24 mW power 325 nm continuous He–Cd laser as an excitation source and a photodiode system for detection at room temperature. The PL measurement was carried out for the ZnO NRs grown on the planar Si and SiMP arrays. The current–voltage (I–V) characteristics of the ZnO NRs/p-Si heterojunctions were measured using a semiconductor parameter analyzer (HP-4155). An external mechanical force was applied to the PNG device by a strain system consisting of a cylinder with a diameter of 0.5 cm, which repeatedly hit the PNG surface, to apply a mechanical compressive force of 0.5 kgf to the PNGs.[24] If the amount of applied mechanical force is constant, the generated output voltage would be decreased with increasing the diameter of the straining rod because the output voltage is inversely proportional to the area of the PNG applying the strain. We varied the applied input frequency over a range from 1.5 to 7.5 Hz to observe the output performance of the ZnO NR/SiMP heterojunction PNGs with respect to the applied frequency. Under periodically applied compressive stress, the output voltage of the PNGs was characterized by an oscilloscope. A higher sampling rate oscilloscope was used to record the output voltage from the device to determine the high-frequency strain rate. All measurements were performed in a faraday cage to avoid external noises from environment.

3. RESULTS AND DISCUSSION

Figure 2a,b shows cross-sectional scanning electron microscope (SEM) images of the SiMP arrays fabricated by etching for 5 and 10 min, respectively. As the etching time increases, the

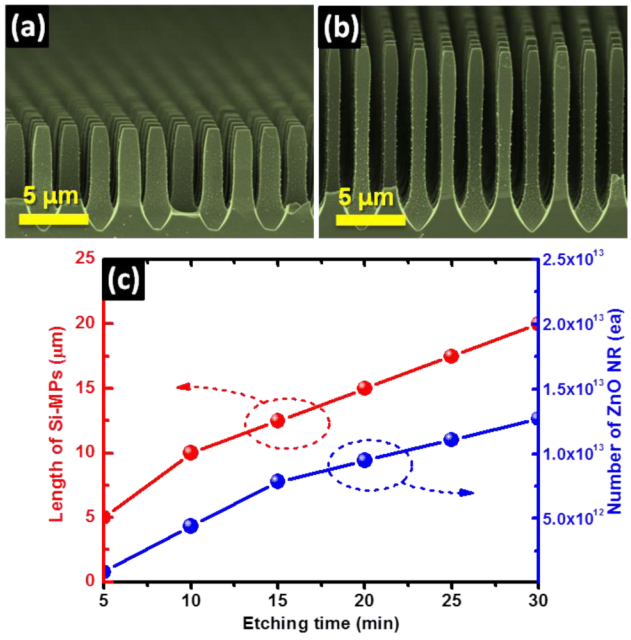

Figure 2. Cross-sectional SEM images for SiMPs fabricated using (a) 5 and (b) 10 min of electrochemical etching. (c) Length of SiMPs and number of ZnO NRs vs electrochemical etching time for SiMPs.

DOI: 10.1021/am5085379
ACS Appl. Mater. Interfaces 2015, 7, 5768–5774

shape of the SiMP changes, while the density of the SiMP arrays remains constant at 2.5 × 10^3 MPs/cm^2 because the photomask pattern was same. The length of the SiMPs was increased linearly from 5 to 20 μm, and the diameter of individual SiMP was linearly changed from 1.2 to 1.02 μm with increasing the electrochemical etching time from 5 to 30 min as shown in Figure 2c. We prepared SiMP arrays with lengths of 5, 10, 12.5, 15, 17.5, and 20 μm by controlling the etching rate and time. It was difficult to fabricate the SiMPs longer than 20 μm using electrochemical etching (see Figure S1 in Supporting Information for more details) and to coat the reliable and uniform PDMS layer. SiMP arrays were formed on a circular area of the Si substrate with a diameter of 2.5 cm for all samples. The ZnO NRs were grown only in this area by selectively forming the ZnO seed layers. As the length of the SiMP was increased, the effective surface area for growth of the ZnO NRs increased, which also resulted in an increase in the number of ZnO NRs.

Figure 3a,b shows cross-sectional and top view images of the ZnO NRs grown on the 10 μm length SiMP arrays,

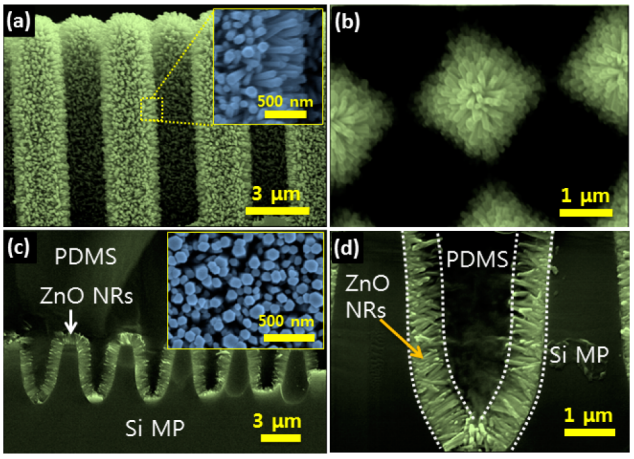

Figure 3. (a) Cross-sectional and (b) top view images of ZnO NRs grown on SiMP arrays with a length of 10 μm. (c, d) Cross-sectional SEM images of PNG device structure, which confirms that PDMS penetrates into the SiMP arrays. (inset a, c) The ZnO NR-grown SiMP and flat Si substrate, respectively.

respectively. ZnO NRs of uniform shape were successfully grown, even on the long SiMP arrays. The ZnO NRs were well-aligned vertically and were perpendicular to the Si surfaces. The ZnO NRs showed faceted six-sided surfaces and a hexagonal top facet, as shown in the inset of Figure 3a. This indicates that the ZnO NRs are wurtzite-structured single crystals grown along the [0001] direction.[23] The inset of Figure 3c shows a plane-view image of the ZnO NRs on a flat Si substrate. The diameter and areal density of the ZnO NRs are estimated to be 105 nm and 1.8 × 10^{11} NRs/cm^2, respectively. We estimated the number of ZnO NRs on the circular area with a diameter of 2.5 cm in the Si substrate by considering the SiMP to be a cylindrical shape. The diameters and lengths of the SiMPs measured from the SEM images. The density of the SiMP was assumed to be the same for all samples because the same mask pattern was used during the photolithography process for fabrication of the SiMP. The areal density of the ZnO NRs was assumed to be 1.8 × 10^{11} NRs/cm^2, which was measured on the flat Si substrate. As shown in Figure 2c, the number of ZnO NRs within the circular area increased greatly from 8.84 × 10^{11} NRs for a flat Si to 1.43 × 10^{13} NRs for a SiMP with a length of 20 μm. Figure 3c,d shows the cross-sectional images of the full structure of PNG. The figures indicate that the PDMS penetrated into the gaps between the SiMPs and made contact with the ZnO NRs. In our device structure, the PDMS plays a critical role in uniformly distributing the applied mechanical stress to the ZnO NRs and in transferring the generated electric field from the ZnO NRs to the outer electrode. In addition, as an insulating material, PDMS prevents an undesirable piezoelectric screening effect by blocking the generation of free electrons between the metal and dielectric interface.[25,26] The PDMS insulating layer also serves not only as a protection layer that prevents electrical shorts created by residues produced during the hydrothermal growth of ZnO NRs but also as a gate that prevents the direct flow of electrons through the external electrode by creating a Schottky barrier.[27] PDMS also improves the effective contact area with the NRs by decreasing contact resistance and makes the combination of the Holmes and Sharvin resistance equation valid in the nanoscale.[28−30] Finally, the PDMS layer acts as a stress diffuser that dispenses the applied force axially.[19]

Figure 4 shows the PL spectra of the ZnO NRs grown on the SiMPs with different lengths that were measured at room

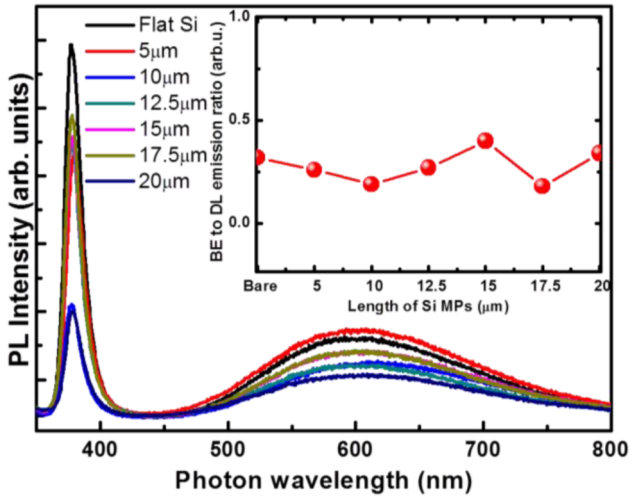

Figure 4. PL spectra measured at room temperature for ZnO NRs grown on SiMP with different lengths. (inset) The band-edge emission to deep-level emission ratio vs the length of the SiMPs.

temperature. The PL spectra show a sharp peak at 375 nm and relatively weak and broader visible emission bands. The peak at 375 nm is assigned to the band-edge emission of ZnO NRs. The broad visible emission bands are the deep levels. In the solution growth of ZnO nanostructures, broad deep-level emission generally prevails over free exciton-related emission.[31,32] Deep-level emission peaks are normally originated from defects such as zinc interstitials, oxygen vacancies, and their complexes in the ZnO crystal.[31−33] Therefore, the PL peak intensity ratio between the band-edge to deep-level emission implies relative amounts of crystalline defects and defect-induced free charge carriers.[25−27] The inset of Figure 4 shows the band-edge to deep-level emission ratio for each sample. The ratio shows almost similar values between 0.2 and 0.3 for the ZnO NRs on flat Si and SiMP substrates, respectively, regardless of the length of the SiMPs. This result indicates that the crystalline quality of the individual ZnO NRs

DOI: 10.1021/am5085379
ACS Appl. Mater. Interfaces 2015, 7, 5768−5774

is not strongly affected by the surface morphology of the underlying substrate. In charge-generating PNG devices, the charge carriers generated by these point defects are detrimentally affected by screening the generated piezoelectric potential and by carrying the charges through the external load.[34,35] This indicates that the crystalline quality of the ZnO NRs on SiMP arrays of different lengths is almost similar for all samples that will be used for PNG applications.

Figure 5a shows the $I-V$ behaviors of the ZnO NRs/p-Si heterojunction, which were measured under dark conditions at

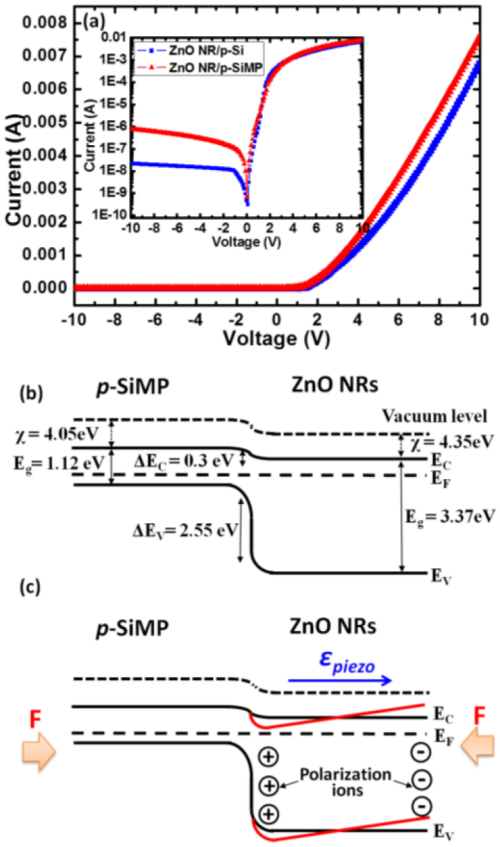

Figure 5. (a) $I-V$ characteristics of ZnO NRs/p-SiMP heterojunctions. (b) Band diagram of ZnO NRs/p-SiMP heterojunction without external force and (c) with compressive stress (red line).

room temperature. Two heterostructured ZnO NR/planar p-Si and ZnO NR/p-SiMP array configurations were prepared by using Ag (100 nm) and Al (100 nm) metal layers for the ZnO NR and p-Si electrodes, respectively. The $I-V$ results clearly show rectifying behaviors for both samples. However, the ZnO NR/p-SiMP structure showed larger leakage current compared to the ZnO NR/planar p-Si structure. This would be attributed mainly from the larger defect or trap centers at the interface of ZnO NR/p-SiMP (see Figure S2 in Supporting Information for more details). An ideal band diagram for the ZnO NR/p-SiMP heterojunction is illustrated in Figure 5b. Here, the ZnO NR was regarded as an n-type semiconductor because of free charge carriers induced by various point defects as discussed in the PL results. The conduction band (ΔE_c) and valence band offsets (ΔE_v) are 0.3 and 2.55 eV, respectively. Because of the larger ΔE_v than ΔE_c, the energetic barrier for electrons is much lower than that for holes. As shown in Figure 5c, when a stress is applied to the ZnO NR side, positive piezoelectric potential is generated at the ZnO NR/SiMP interface. The positive piezo charges at the interface make a trench in the depletion region due to the local piezo-potential. Also, this piezo potential tends to raise the local band and introduce a slope to the band structure (red line). The presence of a carrier-free zone can significantly enhance the piezoelectric effect, because the piezocharges will be mostly preserved without being screened by local residual-free carriers.

Figure 6a–d shows the output voltage measured from the ZnO NR-based PNGs on flat Si-substrate and SiMP arrays with

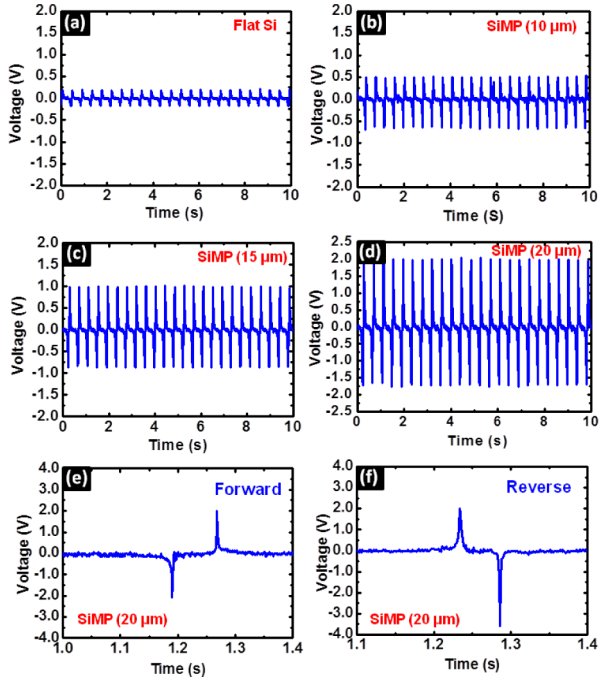

Figure 6. (a–d) Output voltage measured from ZnO NRs on flat Si-substrate and SiMP arrays with a length of 10, 15, and 20 μm with a strain frequency of 2.2 Hz. Polarity-dependent output voltage for (e) forward and (f) reverse connection, which were measured from the PNG on SiMP arrays with a length of 20 μm, respectively.

lengths of 10, 15, and 20 μm, with a strain frequency of 2.2 Hz. The peak voltages from the PNGs on SiMPs were significantly enhanced compared to the 0.7 V obtained from the PNG on a flat Si substrate. All the PNGs showed negative and positive peaks when pushed and released because of charging and discharging, respectively. When a piezoelectric ZnO NR is subjected to an external mechanical force perpendicular to the top surface, a piezoelectric potential is generated along the NRs due to the relative displacement of cations with respect to anions under uniaxial strain. As the strain is applied, a negative piezoelectric potential is generated at the top of the ZnO NRs, which generate the negative potential at the top electrode across the PDMS insulating polymer layer, resulting in a negative pulse. As the strain is released, the piezoelectric potential immediately vanishes, and the carriers accumulated at the top Au electrode flow back through the external circuit to the bottom Au electrode. This causes a positive pulse and returns the system to its original state, as shown in Figure 6a–d. The ZnO NR/SiMP-based PNG device produces alternating current (AC) output signals. This is due to the existence of the PDMS, which acts as a stress diffuser and transfers the stress perpendicularly to the individual ZnO NRs in the PNGs. ZnO-based PNGs generate AC power when the force is

DOI: 10.1021/am5085379
ACS Appl. Mater. Interfaces 2015, 7, 5768–5774

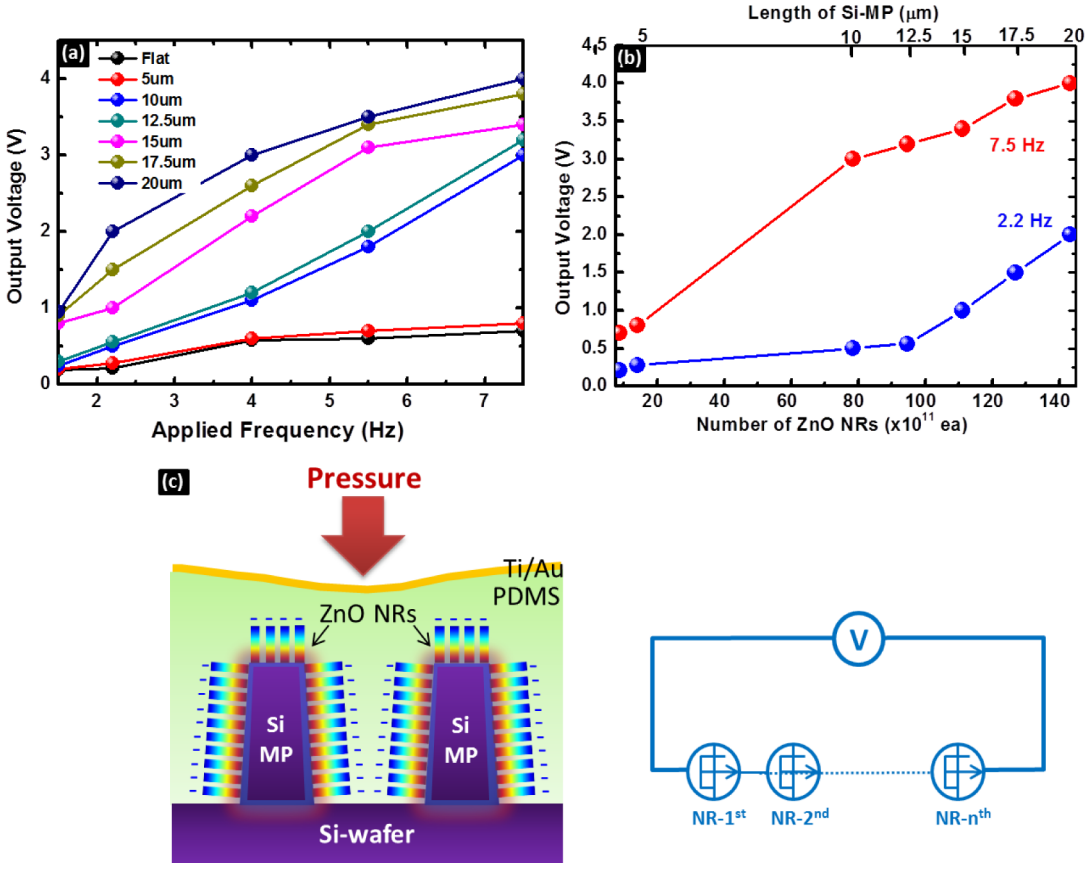

Figure 7. (a) Output voltage of the PNGs prepared on SiMP with different lengths vs applied strain frequency. (b) Output voltage of PNGs depending on the number of ZnO NRs and length of the SiMPs with frequency of 2.2 and 7.5 Hz. (c) Schematic of device structure and simplified equivalent circuit showing working principle of the PNGs.

perpendicular to the vertically grown ZnO NRs.[36] A switching polarity test of the PNG devices was conducted for forward and reverse connections to confirm that the measured signals are originated from the piezoelectric unit rather than from the measurement system. As shown in Figure 6e,f, the sequence of positive and negative output voltage pulses corresponds to the forward and reverse connections. This indicates that the output signals are generated by the PNG itself.

Figure 7a shows the results for peak voltage values versus the applied strain frequency for the ZnO NR/SiMP PNGs for different lengths of SiMPs. As the frequency of the applied stress increased from 1.5 to 7.5 Hz, the output voltage from all the PNG devices increased gradually. As the length of the SiMPs increased, the peak voltage increased to 4 V for the 20 μm SiMP. The increase of the output voltage with increased applied strain frequency has been attributed to the accumulated residual charges. These charges are accumulated by an imperfection of neutralization due to rapid external mechanical stress cycles, resulting in an increase in the piezoelectric potential.[30] Therefore, a larger generated piezoelectric potential causes more carriers to accumulate, and to be released and neutralized. This increases the output voltage by increasing the applied strain frequency for PNGs on longer SiMPs. Figure 7b shows the peak voltage from the PNG versus the length of SiMPs with a frequency of 2.2 and 7.5 Hz, that is, the number of ZnO NRs. Note that the gap between the output voltages for low and high strain rate with increasing the SiMP length. In our ZnO NR/SiMP PNG structures, the output voltage is linearly enhanced with increasing SiMP length at low strain frequency. However, the increase of output voltage is gradually reduced for the longer SiMP structures at high strain frequency. We suggest that the slow increase of the output voltages at high strain rate is due to the increased charge trap states in the longer SiMPs. When the electrical charges transport through the longer SiMP PNG structures under high frequency strain, they can be mostly captured at the trap states resulting in the reduction of output voltages compared to low frequency. As shown in Figure 7a, the gradual increase of the output voltage with increasing strain frequency for longer SiMP (>12.5 μm) supports our suggestion. Even though we experienced the tradeoff between the increase of output voltage and SiMP length, the output voltage is mostly enhanced by increasing the number of ZnO NRs grown on long SiMP. When a compressive stress is applied to the ZnO NRs/SiMP PNG surface, piezoelectric potentials are generated from each ZnO NR, as shown in Figure 7c. A single ZnO NR can be regarded as a single nanogenerator. The maximum piezoelectric potential generated from the surface of a single ZnO NR under external mechanical forces can be expressed as $V_{max} \approx \pm 27(D/L)^3 y_m$, where D and L denote the diameter and length of the ZnO NR, respectively, and y_m is the lateral displacement of the tip of the ZnO NR.[37,38] This equation implies that the piezoelectric potential generated from each ZnO NR would be the same and directly proportional to the maximum deflection at the tip if the aspect ratio of the ZnO NR is uniform. In our structure, each ZnO NR, as a single nanogenerator, is electrically connected in series on the SiMPs as shown in Figure 7c. Therefore, as the length of the SiMP increases, the number of series-connected nano-

DOI: 10.1021/am5085379
ACS Appl. Mater. Interfaces 2015, 7, 5768−5774

generators increases continually and finally results in an increase of the output voltage.[33] Considering the number of ZnO NRs, the output voltage from a single ZnO NR on the 20 μm SiMP is estimated to be 2.7×10^{-13} V, and this value is 2.9 times smaller as compared to the output voltage of 7.9×10^{-13} V for the PNG on a flat Si. The decrease in the output voltage from a single ZnO NR on the longer SiMPs is attributed to the larger charge trap state in the ZnO NR/p-SiMP heterojunctions and inefficient delivery of the mechanical strain through the deep SiMP. This would lead to lower built-in potential in the depletion region while increasing the piezo-charge screening effect. Nevertheless, the output voltage from the whole PNG was enhanced by introducing a SiMP array with longer length due to the greatly increased ZnO NR density. This suggested structure can be a promising approach to enhance the output power of PNGs for driving the Si-based microelectronics.

4. CONCLUSIONS

In summary, we demonstrated the enhancement of output voltage from ZnO-based PNGs by making heterojunctions on SiMP arrays of different lengths. The lengths of the SiMP arrays, which were fabricated by electrochemical etching, were increased systematically by controlling the etching time. The structural and optical investigations showed that the ZnO NRs were grown hierarchically on SiMPs, and their crystalline quality was similar regardless of the length of the SiMPs. As the length of the SiMPs increased, the number of ZnO NRs acting as a single nanogenerator increased, and the output voltage increased. This enhancement of the output voltage is mainly attributed to an increase in the number of series-connected ZnO NR-based nanogenerator by increasing the length of the SiMPs. These results indicate that we can control the amount of voltage generated from the PNG to power small-scale electronic devices that run with different voltages. Especially, the ZnO NR/SiMP heterojunction can be regarded as a promising piezoelectric device, providing high potential for Si-based electronic devices, and self-powered high performance PNGs.

■ ASSOCIATED CONTENT

Ⓢ Supporting Information

TEM results and fabrication of longer SiMPs. This material is available free of charge via the Internet at http://pubs.acs.org.

■ AUTHOR INFORMATION

Corresponding Authors

*Phone: +82538103093. Fax: +82538104770. E-mail: ikpark@ynu.ac.kr. (I.K.P.)

*E-mail: jaehyun@dgist.ac.kr. (J.H.K.)

Author Contributions

§These authors contributed equally to this work.

Notes

The authors declare no competing financial interest.

■ ACKNOWLEDGMENTS

This research was supported by the Basic Science Research Program (Nos. 2012R1A1A1001711 and 2014R1A2A1A11054154) through the National Research Foundation of Korea and by the DGIST R&D Program (No. 14-EN-01) funded by the Ministry of Science, ICT, and Future Planning of the Korean government.

■ REFERENCES

(1) Wang, Z. L. Self-Powered Nanotech. *Sci. Am.* **2008**, *298*, 82−87.

(2) Hu, Y.; Zhang, Y.; Xu, C.; Lin, L.; Snyder, R. L.; Wang, Z. L. Self-Powered System with Wireless Data Transmission. *Nano Lett.* **2011**, *11*, 2572−2572.

(3) Wang, Z. L.; Wu, W. Nanotechnology-Enabled Energy Harvesting for Self-Powered Micro-/Nanosystem. *Angew. Chem., Int. Ed.* **2012**, *51*, 11700−11721.

(4) Wang, Z. L. Toward Self-Powered Sensor Networks. *Nano Today* **2010**, *5*, 512−514.

(5) Lee, M.; Bae, J.; Lee, J.; Lee, C. S.; Hong, S.; Wang, Z. L. Self-Powered Environmental Sensor System Driven by Nanogenerator. *Energy Environ. Sci.* **2011**, *4*, 3359−3363.

(6) Sun, C. L.; Shi, J.; Bayerl, D. J.; Wang, X. D. PVDF Microbelts for Harvesting Energy from Respiration. *Energy Environ. Sci.* **2011**, *4*, 4508−4512.

(7) Zhang, Y.; Yang, Y.; Wang, Z. L. Piezo-phototronics Effect on Nano/Microwire Solar Cells. *Energy Environ. Sci.* **2012**, *5*, 6850−6856.

(8) Wang, Z. L.; Song, J. H. Piezoelectric Nanogenerators Based on Zinc Oxide Nanowire Arrays. *Science* **2006**, *312*, 242−246.

(9) Liu, J.; Wu, W.; Bai, S.; Qin, Y. Synthesis of High Crystallinity ZnO Nanowire Array on Polymer Substrate and Flexible Fiber-Based Sensor. *ACS Appl. Mater. Interfaces* **2011**, *3*, 4197−4200.

(10) Lin, L.; Jing, Q. S.; Zhang, Y.; Hu, Y. F.; Wang, S. H.; Bando, Y.; Han, R. P. S.; Wang, Z. L. An Elastic-Spring-Substrated Nanogenerator as an Active Sensor for Self-Powered Balance. *Energy Environ. Sci.* **2013**, *6*, 1164−1169.

(11) Hu, Y.; Lin, L.; Zhang, Y.; Wang, Z. L. Replacing a Battery by a Nanogenerator with 20 V Output. *Adv. Mater.* **2012**, *24*, 110−114.

(12) Sohn, J. I.; Jung, Y. I.; Baek, S.-H.; Cha, S.; Jang, J. E.; Cho, C.-H.; Kim, J. H.; Kim, J. M.; Park, I. K. A Low Temperature Process for Phosphorous Doped ZnO Nanorods via a Combination of Hydrothermal and Spin-On Dopant Methods. *Nanoscale* **2014**, *6*, 2046−2051.

(13) Kim, H.; Kim, S. M.; Son, H.; Kim, H.; Park, B.; Ku, J.; Sohn, J. I.; Im, K.; Jang, J. E.; Park, J. J.; Kim, O.; Cha, S. N.; Park, Y. J. Enhancement of Piezoelectricity via Electrostatic Effects on Textile Platform. *Energy Environ. Sci.* **2012**, *5*, 8932−8936.

(14) Yan, H.; He, R.; Pham, J.; Yang, P. Morphogenesis of One-Dimensional ZnO Nano- and Microcrystals. *Adv. Mater.* **2003**, *15*, 402−405.

(15) Lee, K. Y.; Kumar, B.; Seo, J.-S.; Kim, K.-H.; Sohn, J. I.; Cha, S. N.; Choi, D.; Wang, Z. L.; Kim, S.-W. P-Type Polymer-Hybridized High-Performance Piezoelectric Nanogenerators. *Nano Lett.* **2012**, *12*, 1959−1964.

(16) Song, J. H.; Wang, X. D.; Liu, J.; Liu, H. B.; Li, Y. L.; Wang, Z. L. Piezoelectric Potential Output from ZnO Nanowire Functionalized with p-Type Oligomer. *Nano Lett.* **2008**, *8*, 203−207.

(17) Shin, S.-H.; Lee, M. H.; Jung, J.-Y.; Seol, J. H.; Nah, J. Piezoelectric Performance Enhancement of ZnO Flexible Nanogenerator by a CuO-ZnO p-n Junction Formation. *J. Mater. Chem. C* **2013**, *1*, 8103−8107.

(18) Lu, M.-P.; Song, J.; Lu, M.-Y.; Chen, M.-T.; Gao, Y.; Chen, L.-J.; Wang, Z. L. Piezoelectric Nanogenerator Using p-Type ZnO Nanowire Arrays. *Nano Lett.* **2009**, *9*, 1223−1227.

(19) Seol, M.-L.; Choi, J.-M.; Kim, J.-Y.; Ahn, J.-H.; Moon, D.-I.; Choi, Y.-K. Piezoelectric Nanogenerator with a Nanoforest Structure. *Nano Energy* **2013**, *2*, 1142−1148.

(20) Lee, K. Y.; Chun, J.; Lee, J. H.; Kim, K. N.; Kang, N. R.; Kim, J. Y.; Kim, M. H.; Shin, K. S.; Gupta, M. K.; Baik, J. M.; Kim, S. W. Hydrophobic Sponge Structure-Based Triboelectric Nanogenerator. *Adv. Mater.* **2014**, *26*, 5037−5042.

(21) Baek, S. H.; Noh, B. Y.; Park, I. K.; Kim, J. H. Fabrication and Characterization of Silicon Wire Solar Cells having ZnO Nanorod Antifelection Coating on Al-Doped ZnO Seed Layer. *Nanoscale Res. Lett.* **2012**, *7*, 29−32.

(22) Noh, B. Y.; Baek, S. H.; Jung, Y. I.; Kim, J. H.; Park, I.-K. Surface Plasmon-Enhanced Light-Emission Mechanism of Ag-Coated ZnO/

DOI: 10.1021/am5085379
ACS Appl. Mater. Interfaces 2015, 7, 5768−5774

Al_2O_3 Core/Shell Nanorod Structures. *J. Nanosci. Nanotechnol.* **2013**, *13*, 3335−3340.
(23) Jung, Y. I.; Noh, B. Y.; Lee, Y. S.; Baek, S. H.; Kim, J. H.; Park, I. K. Visible Emission from Ce-doped ZnO Nanorods grown by Hydrothermal Method without a Post Thermal Annealing Process. *Nanoscale Res. Lett.* **2012**, *7*, 43−46.
(24) Nam, G. H.; Baek, S. H.; Cho, C. H.; Park, I. K. A Flexible and Transparent Graphene/ZnO Nanorod Hybrid Structure Fabricated by Exfoliating a Graphite Substrate. *Nanoscale* **2014**, *6*, 11653−11658.
(25) Lee, K. Y.; Kumar, B.; Seo, J. S.; Kim, K. H.; Sohn, J. I.; Cha, S. N.; Choi, D.; Wang, Z. L.; Kim, S. W. P-Type Plymer-Hybridized high-Performance Piezoelectric Nanogenerators. *Nano Lett.* **2012**, *12*, 1959−1964.
(26) Zhu, G.; Wang, A. C.; Liu, Y.; Zhou, Y. S.; Wang, Z. L. Functional Electrical Stimulation by Nanogenerator with 58 V Output Voltage. *Nano Lett.* **2012**, *12*, 3086−3090.
(27) Yang, R. S.; Qin, Y.; Dai, L. M.; Wang, Z. L. Power Generation with Laterally Packaged Piezoelectric Fine Wires. *Nat. Nanotechnol.* **2009**, *4*, 34−39.
(28) van den Heever, T. S.; Perold, W. J. The Performance of Nanogenerators Fabricated on Rigid and Flexible Substrates. *Microelectron. Eng.* **2013**, *112*, 41−45.
(29) Mikrajuddin, A.; Shi, F. G.; Kim, H. K.; Okuyama, K. Size-Dependent Electrical Constriction Resistance for Contacts of Arbitrary Size: from Sharvin to Holms Limits. *Mater. Sci. Semicond. Process.* **1999**, *2*, 321−327.
(30) Baek, S. S.; Fearing, R. S. Reducing Contact Resistance using Compliant Nickel Nanowire Arrays. *IEEE Trans. Compon. Packag. Technol.* **2008**, *31*, 859−868.
(31) Kim, D. H.; Lee, S. D.; Kim, K. K.; Park, G. S.; Lee, J. M.; Kim, S. W. Free-Standing ZnO Nanorods and Nanowalls by Aqueous Solution Method. *J. Nanosci. Nanotechol.* **2008**, *8*, 4688−4691.
(32) Greene, L. E.; Law, M.; Goldberger, J.; Kim, F.; Johnson, J. C.; Zhang, Y.; Saykally, R. J.; Yang, P. Low-Temperature Wafer-Scale Production of ZnO Nanowire Arrays. *Angew. Chem., Int. Ed.* **2003**, *42*, 3031−3034.
(33) Li, D.; Leung, Y.; Djurišić, A.; Liu, Z.; Xie, M.; Shi, S.; Xu, S.; Chan, W. Different Origins of Visible Luminescence in ZnO Nanostructres Fabricated by the Chemical and Evaporation Methods. *Appl. Phys. Lett.* **2004**, *85*, 1601−1603.
(34) Choi, M. Y.; Choi, D.; Jin, M. J.; Kim, I.; Kim, S. H.; Choi, J. Y.; Lee, S. Y.; Kim, J. M.; Kim, S. W. Mechanically Powered Transparent Flexible Charge-Generating Nanodevices with Piezoelectric ZnO Nanorods. *Adv. Mater.* **2009**, *21*, 2185−2189.
(35) Sohn, J. I.; Cha, S. N.; Song, B. G.; Lee, S.; Kim, S. M.; Ku, J. Y.; Kim, H. J.; Park, Y. J.; Choi, B. L.; Wang, Z. L.; Kim, J. M.; Kim, K. Engineering of Efficiency Limiting Free Carriers and an Interfacial Energy Barrier for an Enhancing Piezoelectric Generation. *Energy Environ. Sci.* **2013**, *6*, 97−104.
(36) Park, H.-K.; Lee, K. Y.; Seo, J.-S.; Jeong, J.-A.; Kim, H.-K.; Choi, D.; Kim, S.-W. Charge-Generating Mode Control in High-Performance Transparent Flexible Piezoelectric Nanogenerators. *Adv. Funct. Mater.* **2011**, *21*, 1187−1193.
(37) Gao, Y.; Wang, Z. L. Electrostatic Potential in a Bent Piezoelectric Nanowire. The Fundamental Theory of Nanogenerator and Nanopiezotronics. *Nano Lett.* **2007**, *7*, 2499−2505.
(38) Song, J.; Wang, X.; Liu, J.; Liu, H.; Li, Y.; Wang, Z. L. Piezoelectric Potential Output from ZnO Nanowire Functionalized With p-Type Oligomer. *Nano Lett.* **2008**, *8*, 203−207.

DOI: 10.1021/am5085379
ACS Appl. Mater. Interfaces 2015, 7, 5768−5774